Egyptian Geophysical Society
EGS Journal, Vol. 18, No. 1, 77-87 (2021)

STRATIGRAPHIC AND STRUCTURAL STUDY WITH INSITU GEOMECHANICAL HORIZONTAL STRESSES DIRECTION FROM WIRELINE WELLBORE IMAGES IN SOUTH SANNAN FIELD, WESTERN DESERT, EGYPT

H. MAHMOUD[(1)], N. ABOU ASHOUR[(2)] and A. SHIBL[(2)]

(1) Petrophysical Data Engineer, Halliburton, (2) Geophysics Department,
Faculty of Science, Ain Shams University, Egypt.

دراسة طبقية وتركيبية بمعرفة الإجهادات الجيوميكانيكية عن طريق تحليل الصور البئرية في حقل ابو سنان الجنوبي بالصحراء الغربية ، مصر

الخلاصة: في هذا البحث، الهدف الرئيسي هو دراسة الضغوط الأفقية القصوى باستخدام المقاومة الكهربائية لصور البئر. كانت البيانات المتاحة ستة آبار، وكلها تستخدم في سير عمل تقني جديد لتحديد اتجاه الترسيب الجيولوجي ثم اتجاه الكسر الجيولوجي ثم اتجاه الإجهاد، كما تم استخدامها لحساب المسامية باستخدام أداة الصورة المقاومة.

إن فهم الطبقات والهيكل والضغط الأفقي الجيوميكانيكي لمنطقة الدراسة سيؤثر على استراتيجيات الحفر المستقبلية للقضاء على مشاكل مثل فقدان سوائل الحفر بسبب الكسور وتقدير خسائر سوائل الحفر قبل حدوثها والاستعداد لحلها في الوقت المناسب ، كما أنه سيساعد في تحديد أفضل اتجاه لحفر بئر أفقي للتطوير المستقبلي.

ABSTRACT: *Due to the location of South West Sannan field, on the south of Abu Gharadig basin in the Western Desert, the majority of wells are being drilled, vertical wells to maximize the production and hydrocarbon recovery in the mature reservoirs of the study area. It is of great challenge to drill a high angle well successfully through a such complex structure, tectonic setting and highly stressed shale. The stratigraphic setting of the area possesses significant drilling challenges, that vary widely from reactive shale to stress-related problems.*

The objective of this paper is to investigate, focus and integrate geologic knowledge for a better understanding of the stratigraphy, structure and geomechanical horizontal stress of the study area, in order to estimate new technical approaches to analyze the wireline data specially the Well bore images and select the optimal methods to study the impact of horizontal stresses on the well bore.

Borehole imaging services provide microresistivity images of the formation in water based mud. Borehole imaging is the preferred approach for determining net pay in the sediments of continental and fluvial depositional environments. Visualizing sedimentary features let to define important reservoir geometries reservoir parameters, and the interpretation of image-derived sedimentary dip data which helps to better understand of sedimentary structures. Geomechanical applications of image logs include fracture identification and differentiation of closed and open fractures along with stress analysis and borehole stability determination. Image logs also assist in porosity determination, presence of vugs, cemented nodules, induced fractures, etc.

INTRODUCTION

Geographically the Western Desert comprises of substantial levels slanting seaward, the monotony of the plains is cut by infrequent low questas, the colossal Qattara Depression, Siwa, Bahariya, Dakhla, Kharga Oasis and the Wadi El Natrun hollows. Location map (Fig. 1.)

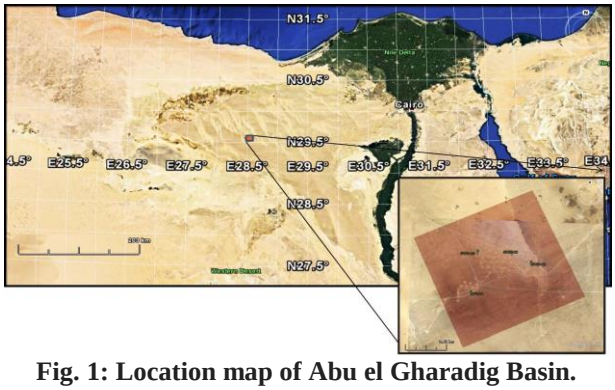

Fig. 1: Location map of Abu el Gharadig Basin.

The sedimentary sequence of the Northern Western Desert of Egypt (Fig. 2) comprises rock units ranging from Cambrian to Recent with the oldest sediments resting on the basement rocks. The litho-stratigraphic column can be subdivided into three sequences according to (Schlumberger, 1984). The first sequence is the lower clastic unit from Cambrian to Cenomanian, then the middle carbonates, from Turonian to Eocene, and finally the upper clastic unit from Oligocene to Recent.

The stratigraphic section of South West Sannan (SWS) field is a part of the stratigraphic sequence of the Western Desert. The stratigraphic sequence of Western Desert covers a sedimentary sequence extenting in age from Pre-Cambrian to Recent.

The generalized stratigraphic sequence at South Sannan field (Fig. 2) rests over the basement complex which consists of Paleozoic, Mesozoic and Cenozoic

rock units. Mesozoic sediments concerned the attention of most of the operating oil companies in this region. However, the majority of the drilled wells at South Sannan field were bottomed in the Cretaceous rocks (Bahariya and Kharita formations).

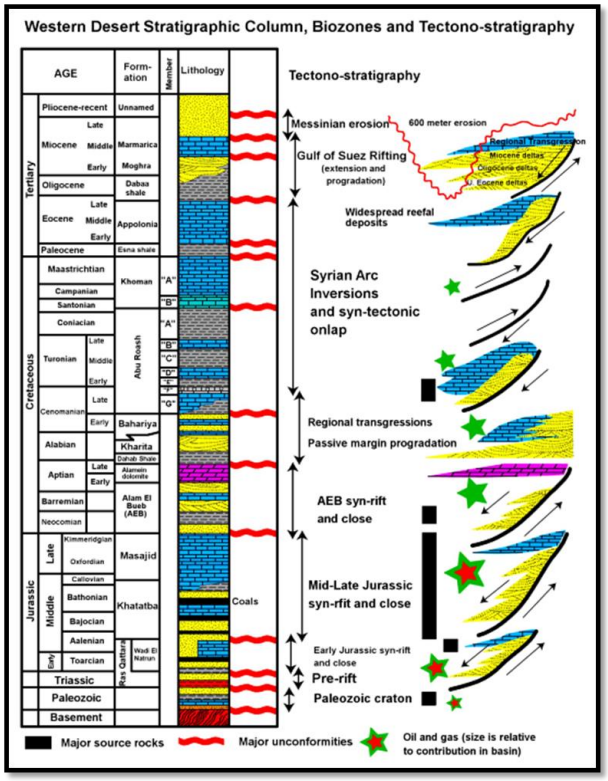

Fig. 2: Stratigraphy log and tectonic episodes, South Sannan field Western Desert, Egypt.(EEPC,2011.)

- Wireline Borehole Geology Images

Borehole image logs span the scale gap between core and seismic observations. Although it does not replace core, provide key sedimentological and sub-seismic structural information, allow quantification of subsurface fracture networks and are inputs to geomechanical and petrophysical studies. These images are typically used to obtain the structural dip of the 21 formation penetrated by wells, identify thinly bedded reservoirs, and analyze fractures and faults, particularly those of small scale below the seismic resolution.

In this study first some of the borehole image features are discussed with examples and then an image log case study is carried out to interpret the reservoir sedimentary environment.

Examples of the geological features from a single well in the Ventura basin, California, contain excellent models of faults (Amer et al., 2011.) We are also able to identify and verify overturned beds and repeat stratigraphic sections in the well because the image logs enable us to document the presence of reverse faults (Fig. 3). Image log interpretation is carried out after running the corrections and enhancements on the measured data. Since the image logs are going to be integrated with the conventional logs, necessary depth matching between the runs is carried out. Fewer corrections are usually implemented on the image logs since often service companies do necessary corrections on the logs before delivery.

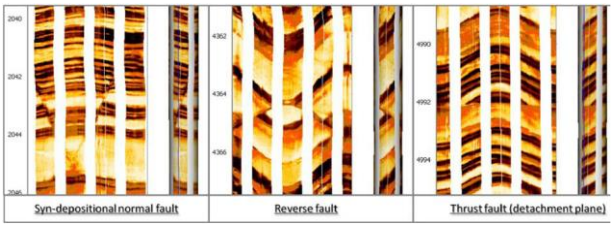

Fig. 3: Normal, reverse and thrust faults as observed on high-resolution image logs (Amer et.al., 2011.)

Borehole image was logged over the interval: 2302-1650 m, in the well HF-35-2X of the Abu Sannan field, located in Western Desert, Egypt. The HF-35-2X well is deviated with a maximum deviation of 5.43 degrees; it was drilled using an 8.5 inch drill bit.

The main reasons for acquiring the Borehole image were for geological evaluation purposes, like: facies characterization and extrapolation to un-cored intervals, enhancing understanding of depositional processes and reservoir geometry using sedimentary dip data, characterization of sub-seismic deformation features (faults, fractures, syn-sedimentary deformation). Image processing and a detailed sedimentological interpretation including electro-facies analysis were performed. Facies association and depositional environment prediction along with a detailed structural interpretation were accomplished over the Kharita, Bahariya and Abu Roash formations spanning the interval 2302-1650 m.

- Depth Matching

Depth matching is done between the Borehole Image log run and the triple combo run. The triple combo run includes the main porosity logs and the GR log. (Fig. 4.) shows the two GR logs one from the triple combo-run comp:GR and another from image log run Well bore Image (WBI):GR_EDTC. The triple combo run is assumed as the reference run in the well and all the other logs depth matched with this run.

According to the plot, there is a need for +0.3m shift to the FMI run GR to match the composite log GR. The amount of the shift, however, is not the same in the whole well interval and changes from zero to about +0.7 meter. It should be noted that the amount of the depth matching shift between the LWD logs versus wireline logs (here we assumed triple combo run) is most of the time different values. This is because the LWD tools are conveyed in the drilling strings while the wireline tools are hanged from wireline cable. Tension in cable and drill pipe is different; therefore the amount of shifting is different. We trust the wireline depth more than LWD due to the cable tension monitoring. But the drill string measurement and human based error increases depth uncertainty.

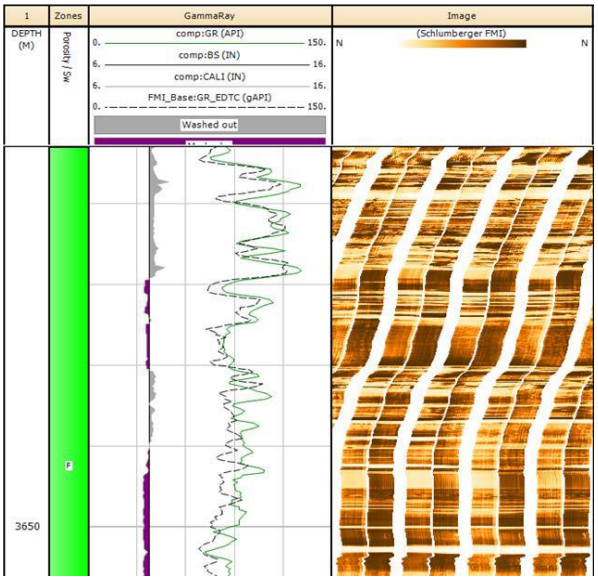

Fig. 4: Comparison between the Triple Combo-GR and WBI-GR logs to check for the logging runs correlation and depth match.

- Dip picking and Sedimentary features

The dips seen on the borehole image logs are as they appear on the surface of a conventional core. The trace of a plane dipping bed forms a sinusoidal curve when the image of the borehole wall is unwrapped and laid flat, as we see in (Fig. 5.) Most of the picking tools generate a pick which can produce a meaningful dip representing the feature identified. A dip is composed of three elements, a depth, an angle, and an azimuth. Plotting a dip alongside the other dips with appropriate display allows trends, boundaries, and patterns to be identified. Bed boundaries, beds, slump features, faults and fractures are easily seen in the image logs.

Logging quality for picking the sedimentary bedding features and structural analysis is also important factor. After logging quality control and acceleration correction to enhance the log quality, there are still some intervals that the image log is not interpretable due to tool stuck and distorted micro resistivity image values.

To pick the dipping traces in the image logs, the logs were already enhanced by log processing. Dips on this case study image log are picked and classified manually. Different dipping features were identified and picked for sedimentary and structural interpretation.

Identified dips are sedimentological and low angle features including, shale and sand bed boundaries, erosion surfaces, unconformities, high angle structural features such as faults, fractures and drilling induced fractures and some other features like nodules, lenticular features and deformations.

Figure (5) illustrates a four meter of the well interval with defined dipping layers. Two sandy beds; one at 1865m depth with 0.6 meter thickness and another at 1867m depth with 0.5 meter thickness. Track four shows the tadpole plot of the dips which display the sinusoid planes on the picked features as the dip angle and dip azimuth. This track shows the dip angle of the picks and the direction of the tadpole tail shows dip azimuth from the North.

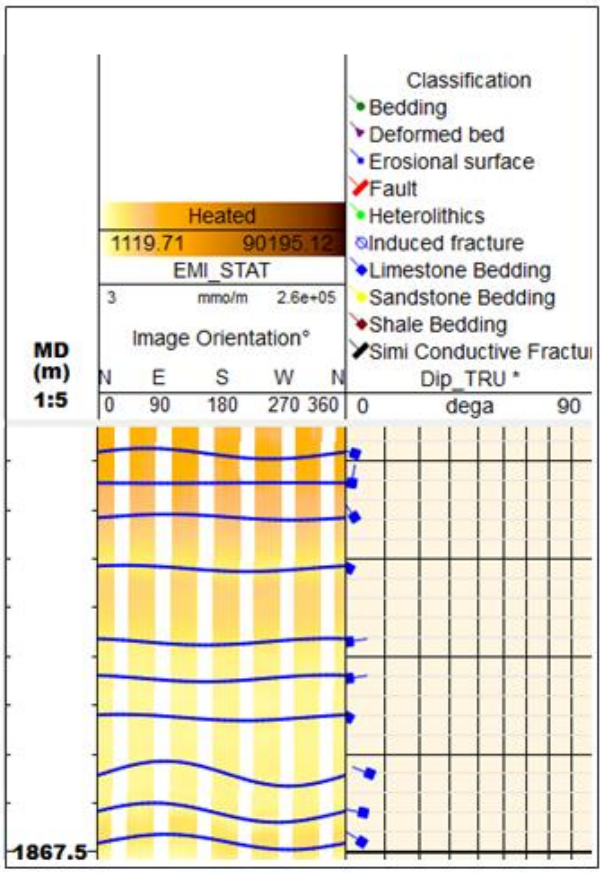

Fig. 5: Borehole Image log with identified features including two sand bed boundaries 5-10 degree with carbonate beds in between sandy layers.

Accordingly, the azimuth of the thin shaly layers is about 180 degree from the North with the dip angle of 5 to 10 degree. However, the sandy layer at the top has slightly higher dip angle of about 13 degree with similar dipping azimuth as shales beneath that sand toward the South.

The sandy layer at the bottom, however, has different dip angle and azimuth. The dip angle of the layer is 25 degree toward the 270 degree from North. The cemented shaly sand layers below the bottom sands show even more dipping layers of about 50 degree toward 270 degree north. In addition to the sedimentological beds and bed boundaries, two drilling induced fractures are seen in the image. These fractures are visible over the shaly and sandy layers indicating that the drilling mud pressure was considerably higher than the formation pressure.

Sedimentary and structural dip features were manually picked using a sliding sinusoid in the WBI module of the Techlog software package. Sinusoids were

fitted to planar or sub-planar features that cut the borehole. The lowest point on the sinusoid trough defines the dip azimuth, and the amplitude of the sinusoid defines the dip magnitude. Dips are presented as magnitude and azimuth in this report, with the following format (magnitude / azimuth – e.g. 10o / 120o).

Sedimentary dips were defined as those resulting through depositional processes and include bed boundaries (e.g. planar bed tops and bases, uneven erosional contacts) and internal bedding features (e.g. internal sand and mud laminations, heterolithic laminations). Structural features include those planes that cut across bedding (e.g. fractures, faults). No obvious structural controls (e.g. faults, fractures and etc.) have been noticed from image.

- Structural Dip Determination

Structural dip is generally defined from bedding in lithologies that are assumed to have been deposited with a horizontal or near-horizontal attitude. This includes bedded or laminated shale and thinly interlaminated (heterolithic) lithologies. HF 35_6, HF 36_5X, HF 35_2X, HF 35_7, HF 35_4, HF 35_11 and SS2 wells were penetrating through vertically tidal channels, transgressive sand bars, and tidal flat deposits. These channelized sandstone and bars are observed from the FMI Schlumberger and XRMI Halliburton images with scour bases.

The studied interval is showing structural dip observed in the HF 35-6, HF 36-5X, HF 35-2X, HF 35-7, HF 35-4, HF 35-11 and SS2 based on the Structural dip zonation determined from manually picked bed boundaries in shale and heterolithics. It shows a dominant NW dip azimuth trend with overall scattering due to a low mean dip magnitude of 2.2 deg which is the reason why only one structural zone is taken. Shales are deposited under quiet depositional conditions from suspension. A low dip angle indicates that the interval has not been affected by any structural element or event. Therefore, no structural dip removal has been performed for any manually picked features (Sand Dip, Heterolithics, Cross Bedding and Flaser Bedding). (Fig. 6 and Fig. 7).

In figure (6) we can see the the main structural dip based on the bed boundaries which are picked over the interpreted intervals in each well of HF 35-6, HF 36-5X, HF 35-2X, HF 35-7, HF 35-4, HF 35-11, SS2. In figure (7) The Stereonet map view for the wells location on the 2D map is showing the main structural dip based on the bed boundaries which are picked over the interpreted intervals in each well of HF 35-6, HF 36-5X, HF 35-2X, HF 35-7, HF 35-4, HF 35-11, SS2. The Main important point is that all the northern five wells show structure dip toward the north with azimuth vary from 250 degrees to 30 degrees while SS2 is completely different with a direction of 150 degrees south east.

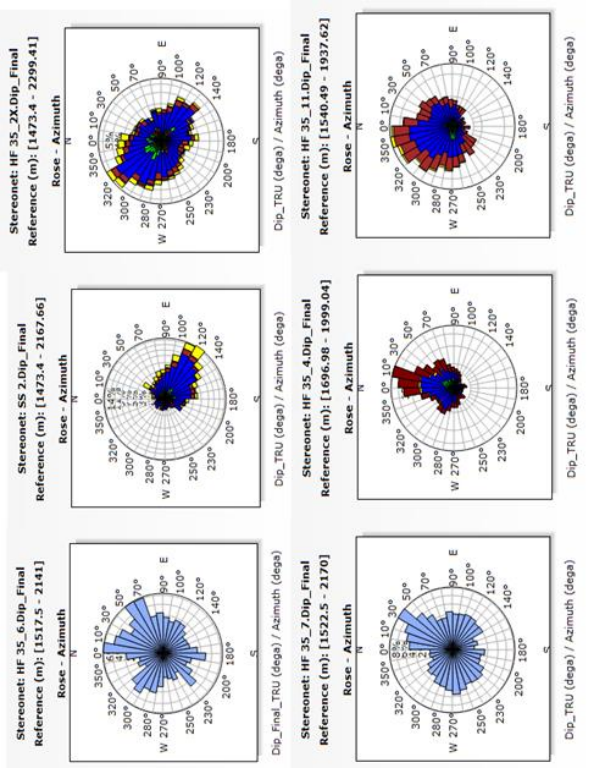

Fig. 6: Stereonet is showing the main structural dip based on the bed boundaries which are picked over the interpreted intervals in wells HF 35-6, HF 36-5X, HF 35-2X, HF 35-7, HF 35-4, HF 35-11, SS2.

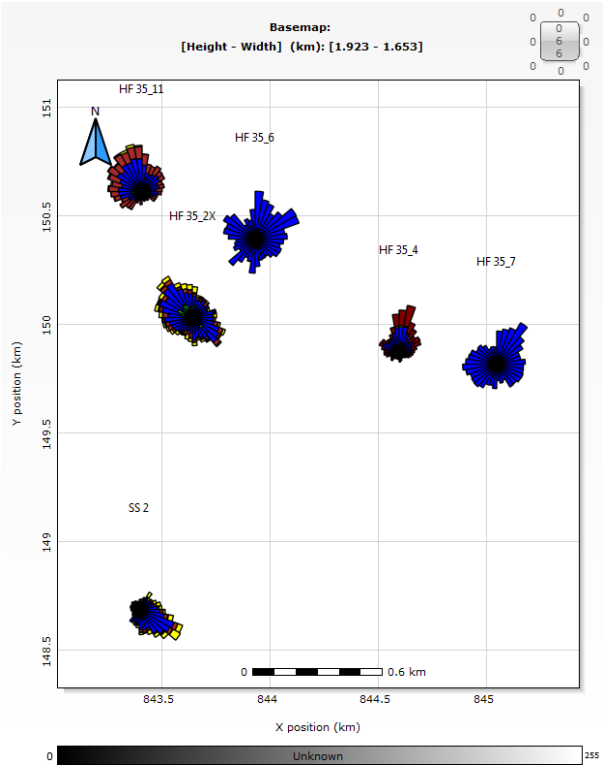

Fig. 7: Stereonet map view for the wells location on the 2D map showing the main structural dip based on the bed boundaries which are picked over the interpreted intervals in wells HF 35-6, HF 36-5X, HF 35-2X, HF 35-7, HF 35-4, HF 35-11, SS2.

- Identified Fractures

In the interpreted interval: 2302-1650 m many dip sets were identified, some of them are sedimentary dips and the others are geostress dips as discussed below:

The sedimentary features are represented by the bedding planes (Bed boundary, sand dip, cross bedding, heterolithics, co-set boundary, flaser bedding and scour surfaces etc.) in this well. The geostress elements been observed in this well are drilling Induced fractures and borehole breakouts.

- Bed Boundries

Bed boundaries were picked for all different lithologies except sandstone units over the requested interval: 1650-2302 m. They show a dominant NW dip azimuth with average dip magnitude of 2.2 deg.

Bed boundaries were used to determine structural dip zones in case removal was needed. This however was not the case since their dip magnitude was low which indicated that no structure was influencing any of the interpreted interval.

- Sedimentary Sand Dips

Sand dips include laminations, cross bedding, cross laminations, wavy bedding, flaser bedding were picked over the requested interval: 2302-1650 m in the sandstone units. The Kharita Formation (2302-2257m) cross-beds and sand dips show a dominant NW-NNW dip azimuth with a subordinate to the NE. The Bahariya Formation (2257-2009m) cross-beds and sand dips show a bi-directional distribution to the NNW and NNE directions because the data was recorded in the Abu Rouash and Baharia formations .

Dips in sand lithology help to determine the direction of paleo-current flow after structural dip removal. Since in this well no structural dip was seen to act on the interval, the overall direction of paleocurrent flow is therefore identified as flowing to the NW from the SE.

- Erosive and Diagenetic Surface

These surfaces include scour surfaces, erosive bases, reactivation surfaces, diagenetic surfaces and transgressive surfaces which were all observed in the sandstone units. The average dip magnitude is 2.1 deg with a scattered dip azimuth.

- GeoStress dips - Induced Fractures

Induced fractures are dominant in brittle lithology and are fractures induced by drilling operations, aligned parallel to the present day maximum horizontal stress orientation in a vertical well. They were picked over the requested interval: 2302-1650 m showing a dominant NW - SE strike orientation (Fig. 7).

- GeoStress dips - Borehole Breakout

These features are dominant in the more ductile formations in which there is some shear failure resulting in borehole ovalization; the direction of the breakouts in this well are mainly NE –SW which represents the direction of the present day minimum horizontal stress (Fig. 8). This means that the maximum horizontal stress is NW-SE in the same direction of the induced fractures.

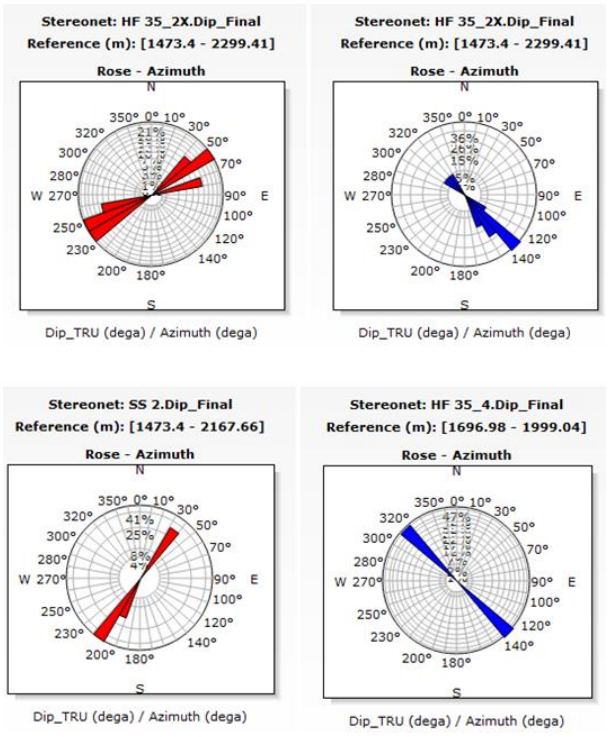

Fig. 8: Rose diagram showing strike orientation of borehole breakouts (left) and drilling induced fractures (right).

- GeoStress Orientation

Borehole electrical images from the wellbore imaging tool with their high resolution and complete full bore coverage provide a detailed picture of the borehole wall. Hence these images can be very efficiently used to identify borehole breakouts and induced fractures and determine their orientations. Borehole breakouts occurring as grooves on the borehole wall, produces a standoff on the measurements done by the sensors/buttons of the imaging tool. Sensors/buttons facing the breakout will read the infilling water based mud and thus show conductive appearance on the image. This conductive feature will appear at diametrically opposite sides of the borehole wall. Such types of conductive features producing a groove like appearance and occurring on opposite sides of the borehole wall were classified as breakouts. Once classified, an elongated sinusoid was then fitted longitudinally along the breakout to determine the directions of the latter.

Induced fractures occur as vertical cracks on opposite sides of the borehole wall. These are formed when the mud weight exceeds the strength, which the rock can withstand and therefore gets fractured. Once fractured the conductive mud enters thereby resulting the dark appearance on image. Induced fractures are different from natural fractures by the fact that the latter are inclined and so have a sinusoidal appearance on the image, whereas the former are vertical and so appear as

elongate cracks. These elongated vertical cracks having conductive appearance and occurring on opposite sides of the borehole wall were classified as induced fractures. Once classified, an elongated sinusoid was then similarly fitted longitudinally along the fracture to determine the directions. Normally induced fractures and borehole breakouts are orthogonal to each other. Hence at any particular depth if the induced fractures are found on pads 1 and 3, breakouts are expected on pads 2 and 4 or vice versa (Fig. 9).

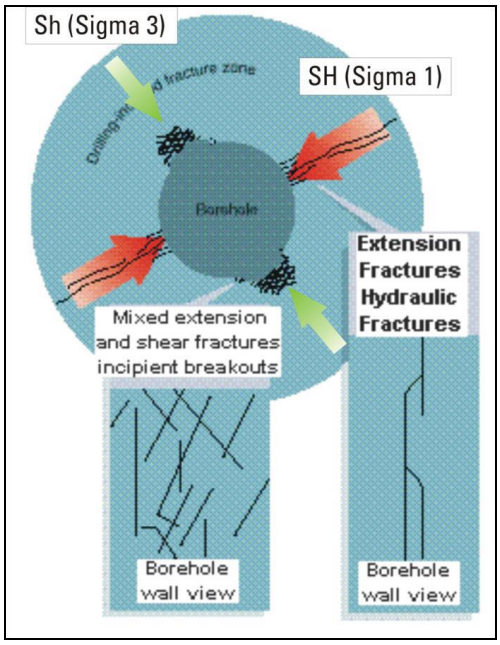

Fig. 9: Borehole Failure resulted in Breakouts and Induced Fractures.

Induced fractures never cross the borehole and they are oriented parallel to the maximum principle stress. Breakouts are basically generated by compressional shear collapse of the formation, and strike along the minimum geostresses direction.

In well HF-35-2X, the strike of the drilling induced fractures is NW – SE which represents the direction of the present day maximum horizontal stress and it has been observed in the brittle lithologies. The strike of the borehole breakouts is toward NE – SW which represents the direction of present day minimum horizontal stress and is well developed in the ductile lithologies (shale).

- Paleo-current Orientation

The sand dips and cross bedded sandstone orientations over the interpreted interval: 1500.16-1997.93 m are summarized in (table 1) including the values of the dip azimuth and mean dip magnitude value for each member. Figure (10) is illustrating the Paleocurrent Zonation results. Also, figure (11) is a very important plot to understand the major paleocurrent. As we see the walk out plot with zone color index shows that the structure dip direction is mainly north from the bottom depth 1997.75 m to the top recorded depth for the sample well 1698.22 m.

Table 1: Paleocurrent Zonation

Structure Dip Removal					
	Zone name	**Top**	**Bottom**	**Dip (dip/azi)**	**Angular error**
1	AR A	1500.16	1528.25	2.5/2.1	2.07
2	AR B	1528.25	1588.00	2.5/2.1	2.07
3	AR C	1588.00	1676.05	2.5/2.1	2.07
4	AR D	1676.05	1762.53	2.9/10.7	1.62
5	AR E	1762.53	1857.91	2.2/352.7	2.23
6	AR F	1857.91	1857.96	2.4/313.5	1.92
7	AR G	1857.96	1997.93	3.3/19.3	1.62

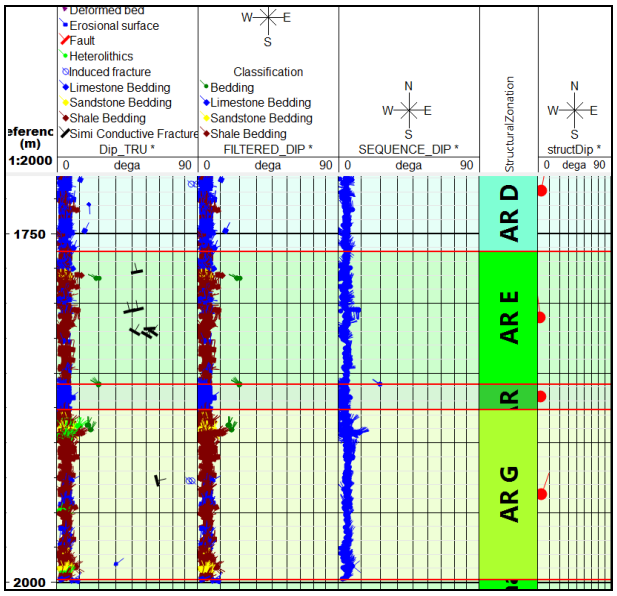

Fig. 10: Paleocurrent Zonation in Each Zone for South West Sannan, Western Desert.

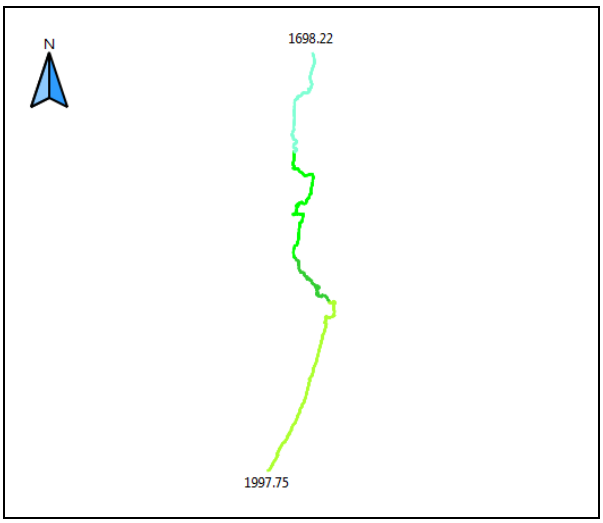

Fig. 11: Walk out plot with zone color index.

- Sedimentological Interpretation

Detailed sedimentological interpretation was performed over the entire study interval, and comprised lithofacies definition from the FMI (Formation Micro Imager) borehole images, packaging of lithofacies into lithofacies associations that are directly related to depositional packages, and then detailed interpretation of these depositional packages in terms of an overall depositional model.

The Borehole images complement the seismic observations, petrophysical evaluation and core interpretation have added finer scale detail to the vertical facies succession and stratigraphic dip changes, and they have enabled identification of significant depositional surfaces.

Sedimentary dip types were used in order to help define lithofacies, depositional packages and to determine paleoslope and paleocurrent orientations. Detailed sequence stratigraphic interpretation was performed because biostratigraphic information was provided and accurate age dating of the sequence penetrated was got from core data interpretation.

Methodology

A. Image Calibration

B. Spectral Analysis

   a. Porosity Spectrum Analysis

   b. Sand Spectrum Analysis

   c. Sand Count

- Image Calibration

The calibration method uses an appropriate calibrated measurement to calibrate borehole image logs, for example calibrating an electrical imaging tool such as the FMI using a resistivity or conductivity variable from a resistivity measuring tool.

The method calculates automatically a best guess calibration using a series of linear regressions, over the response range of the input data, between the calibration variable and the mean value of the input image arrays. You can then edit the best guess calibration by adding or deleting calibration points, and see the results of their changes updated interactively on the screen. When satisfied with the match between the calibration curve and the mean image response, they can apply the calibration to all of the image data.

There are no tool specific transforms included with this first implementation of the method, the calibration will be done without regard to the nature of the image or calibration measurement and will not correct independently for external effects which may impact the image and the calibrated measurement differently such as borehole size or salinity. The calibration process works with zones, as with other, to independently calibrate zone by zone. You can use it to calibrate logs affected by changing borehole conditions or tool response.

All of the input image arrays will be used to compute the mean image response. Therefore, if a particular pad has a poor response it should be excluded before initially running the method. Once the calibration fit is satisfactory it can be added back into the inputs list to have the calibration applied to it. In this way it will not adversely affect the calibration **(Fig. 12)**.

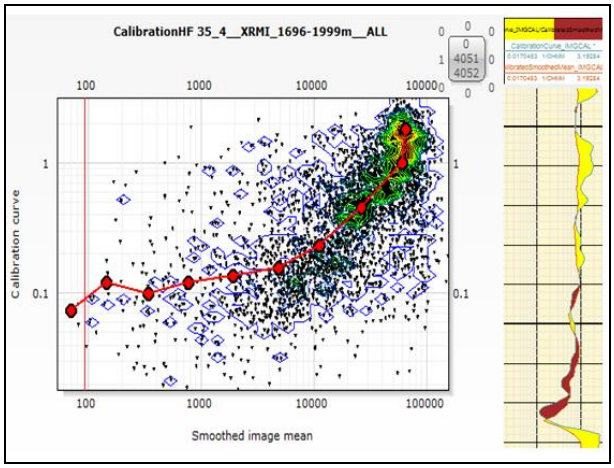

Fig. 12: Calibrating conductive resistivity Image to micro spherical wireline log.

- Porosity Spectral Analysis (PoreSpect)

The PoroSpect (porosity spectrum analysis) method provides porosity distribution and vug fraction quantification from high-resolution electrical borehole images such as formation microImager (FMI) images. The technique is only valid for images acquired in conductive muds.

Many productive carbonate formations have complex dual porosity system consisting of matrix primary porosity and secondary porosity. The secondary porosity might contain vugs, molds or fractures. Borehole electrical conductivity and resistivity images provide both small scale resolution and azimuthal coverage to quantify the heterogeneous nature of the carbonate porosity component. The implementation of PoroSpect supports any calibrated borehole image scaled in conductivity or resistivity. The conductivity or resistivity data from the electrical images is measured in the flushed zone of the borehole (Fig. 13).

In figure (14) and figure (15) The calibrated electrical images are transformed into a porosity map of the borehole using the following equation (MAkbar and Sandeep 2000):

$$\emptyset_i = \emptyset_{log}[R_{LLS} * C_i]^{1/m}$$

Ci: Conductivity of each button from the image

RLLS: External shallow flushed zone resistivity curve

$\emptyset_{log}$: External porosity curve

m: Archie cementation exponent

$\emptyset_i$: Derived porosity for each button of the image

The external resistivity curve must be a shallow resistivity curve reading in the same part of the flushed

zone as the image (for example: **LLS** or **RLA3** for an **FMI**). If such an external curve is also used to calibrate the image, you can also use the average value of the image (for example: **SRES** from image calibration) smoothed to a resolution similar to that of the external porosity curve.

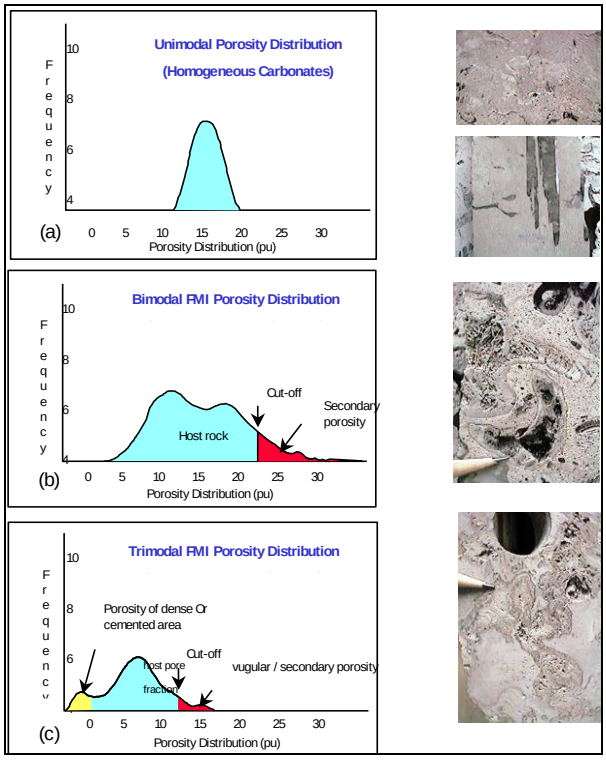

Fig. 13: Typical porosity histogram showing porosity distributions in homogeneous and heterogeneous carbonates. Unimodal distribution is found in homogeneous carbonates: (a) While bimodal to trimodal distributions are found in heterogeneous carbonates. (b&c) The porosity component due to vugs and fractures is obtained by applying an empirical cut off to the porosity histogram.

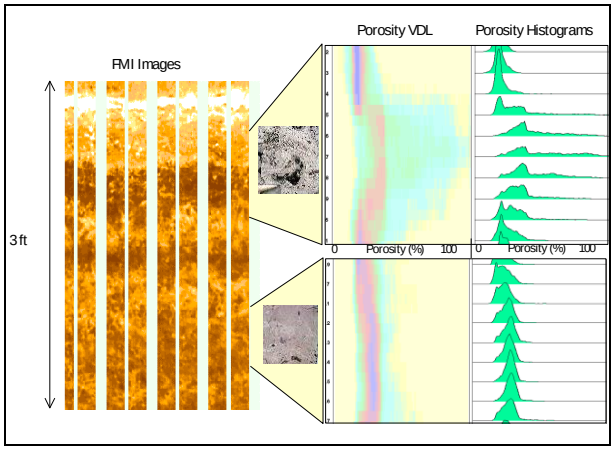

Fig. 14: Two small sections of FMI are transformed into porosity domain, which is shown as porosity histograms and variable density display developed from series of porosity histograms.

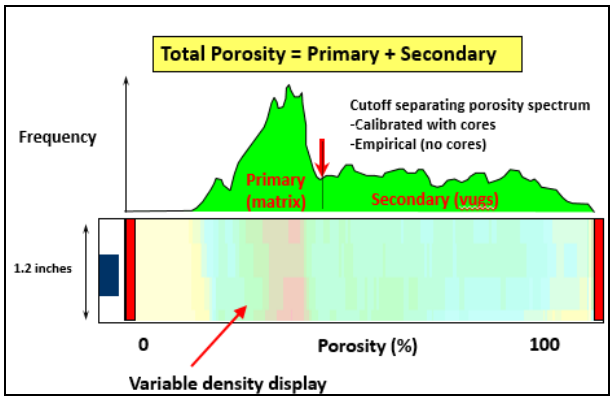

Fig. 15: Reference to MAkbar and Sandeep 2000 the cutoff separation between Primary and secondary porosity.

- Methods

1. WN (William Newberry) Method

In the WN method (Newberry, et al., 2004), a histogram of porosities over a short depth window (1.2" as a default) is computed. The standard deviation (σ) of the histogram below the median porosity is computed and gives an estimate of the threshold. The threshold is obtained by adding a multiple of this standard deviation to the median porosity. As a default, the value of the multiple is taken as 3σ, however this is not fixed. You can increase or decrease it based on the calibration of the porosity results with cores.

2. SDR or Fixed-Percentage Method

This method locates the threshold at a user-defined fixed percentage (default value is 15 %) above the mean porosity. Core observations and measurements provide a way to calibrate this value.

3. TSR (T.S. Ramakrishnan) Discriminant Method

The TSR (Ramakrishna, et al., 2009) method does not require to add any input to define the threshold. It involves decomposing a distribution on linear discriminant analysis (LDA). This method works on the idea that the data are grouped into classes by minimizing within-class scatter and maximizing between-class scatter so that within a group data are similar while between groups they are different. If the porosity data consists of two populations, the best threshold might separate the two means.

4. Gaussian Extraction Optimization-based Method

All the previous methods classify a distribution into disjoint groups. This optimization-based method is designated as JCG (Jaideva C. Goswami) (Goswami, et al., 2004). The approach is the multi-modal decomposition of a composite distribution, applied in this case to the porosity distribution which you can consider as a superposition of several distributions, each corresponding to some type of pore l. The JCG method identifies one of the Gaussian distributions as secondary porosity and computes the secondary porosity by integrating the individual distribution.

Using the SDR the porosity was calculated in figure (16).

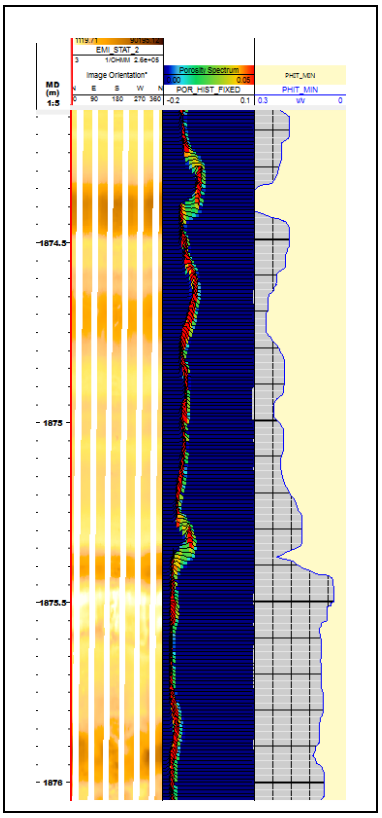

Fig. 16: Porosity calculation using micro Resistivity Image.

- Flattening

If PoroSpect computation was chosen to analyze, its better to read along the bedding direction and not across multiple beds when the bedding is inclined relative to the well. This step requires a dip dataset containing representative bedding dips, with the corresponding apparent dip variables in the flattening parameter tab. The apparent dip variable must have the same orientation reference (north/top of hole) as the borehole image to be flattened.

- Sand Spectrum Analysis (SandSpect)

The SandSpect (resistivity spectrum analysis) method analyses resistivity distribution from calibrated electrical borehole images, such as Formation MicroImager (FMI) or Oil-Based MicroImager (OBMI) images, though histogram and quantile analysis.

The resistivity distribution in images in clastic formations may be related to important textural parameters. The implementation of SandSpect supports any calibrated borehole image scaled in conductivity or resistivity.

Figure (17) Quantile values and a resistivity histogram are computed over a user defined window. The quantile values are used to compute an image sorting Index (SORT). The variations in types of image sorting are similar to the ones seen in grain sorting in clastic rocks and might vary from well sorted, poorly sorted, bimodal to skewed either to low or high end. The sorting index computation used is a simple function of the percentile distribution (Newberry,et al., 2010.)

$$SORT = \frac{70th\ Percentile - 30th\ Percentile}{50th\ Percentile}$$

The upper and lower percentiles used are user defined, 70 and 30 are the defaults. An additional computation looks at the full spread of the data (RSORT = (P99-P01)/P50). The well sorted portion of the resistivity distribution is defined on the resistivity histogram by setting thresholds of 25% of the peak height either side of the peak. Values outside of these thresholds are included in the conductive or resistive fractions and the resistivity of the conductive, well sorted and resistive fractions is computed (Fig. 18).

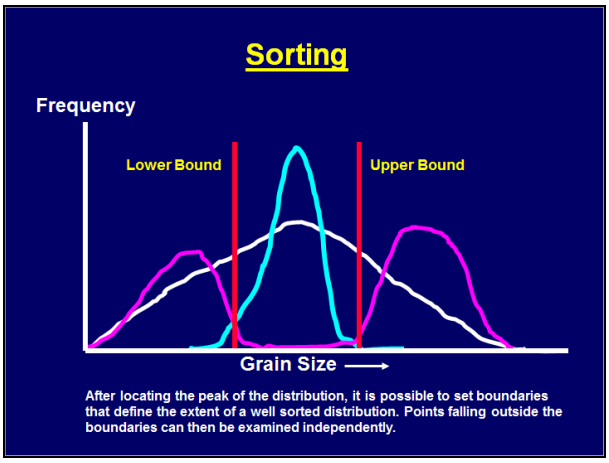

Fig. 17: The basic spectrum distribution analysis for sorting (Newberry et al., 2004).

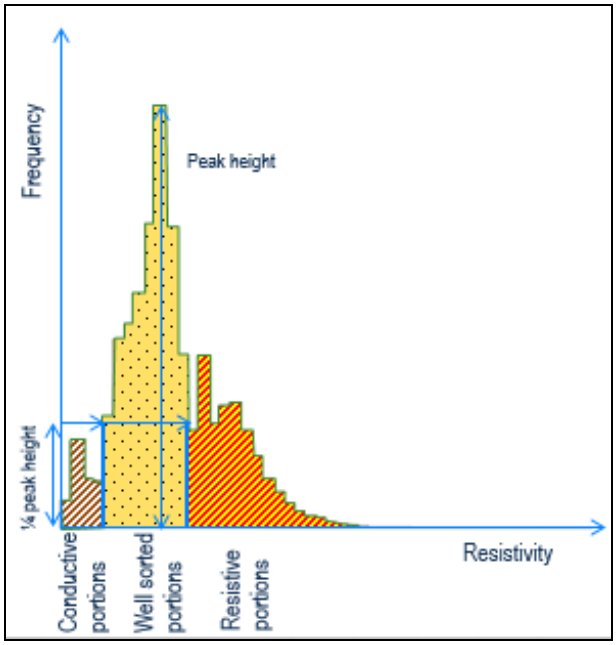

Fig. 18: The histogram distribution classification (After Newberry et al., 2004).

We define the upper and lower percentiles (default is 70th and 30th) the difference is divided by the 50th percentile.

We have to be aware that the sorting does not measure an absolute value of the resistivity, but depends only on the relative spread of the spectrum. The bigger the difference between the upper and lower percentiles the higher the sorting.

Additional percentiles are also computed to get a raw sorting. You can compare the raw sorting with computed sorting to see if you need to change upper and lower limits. From these distributions a peak of the histogram is calculated and the boundaries of a well-sorted distribution are calculated (Fig. 19).

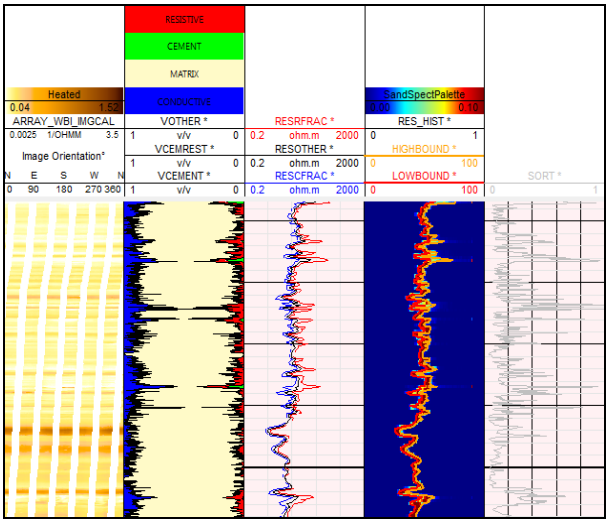

Fig. 19: Sorting in the last track is calculated based on the low and high boundaries picked from the resistivity histogram calculated based on the resistivity image.

The Image sorting index may have a relationship to grain size sorting, but this can only be verified by comparison with core derived data. Nonetheless, the quantitative descriptions of the resistivity distribution that are output by the SandSpect method can contain important information on textural variations.

The WBI images were described in detail on the computer at a scale of 1:10. Grain-size cannot be directly interpreted from the FMI* image and a uniform grain-size was applied to the sandstones. SandTex* histogram results were used for depositional cycle identification and sorting index for the clastic sediments.

Lithofacies and lithofacies associations were defined from the images, with conventional logs. Sedimentary dips were manually picked, and azimuthal plots were generated for the various sedimentary dips within individual depositional packages. These sedimentary dips were interpreted in terms of the overall depositional model and were used to determine structural and depositional dips, where possible. The overall structure of the HF-35-2X well is dipping toward the NW.

Image Based Lithofacies

Individual lithofacies were defined based on detailed description of sedimentary structures from the image logs. Lithofacies are descriptive terms only and should not be taken alone as indicators of depositional environment. In general the development of depositional facies can be considered to be process rather than depositional setting controlled, and similarly the same lithofacies may be developed in more than one depositional setting (as an extreme example cross-bedded sands may develop in fluvial, aeolian, or marine settings).

- Lithofacies Association

Lithofacies associations have a generic relationship to depositional environment and are defined (interpreted) from lithofacies groupings and / or successions. They may be considered as depositional "building blocks" within an individual depositional system (e.g. subtidal muds, tidal channels, tidal bars, shelfal shale and subtidal limestone may all be considered facies associations within a tidal to shallow marine depositional environment). Individual lithofacies associations are commonly dominated and defined by one lithofacies (e.g. meandering river sand lithofacies association is dominated by massive sand lithofacies) but each lithofacies association can also contain a wide variety of lithofacies. This reflects the changing dynamics of deposition within each lithofacies association.

CONCLUSIONS

- The maximum horizontal stress direction is in NW-SE from breakout Sterionet plots around 310 degrees.
- WBI can be a very useful input for estimating sorting, using sand spectrum analysis.
- Porosity can be calculated from the micro resistivity image using image calibration and porosity spectrum analysis.
- Walk out plots indicate the paleocurrent and the major direction of cross bedding in South Sannan is to North.

Acknowledgment

The authors sincerely thank the management of the Egyptian general Petroleum Corporation (EGPC) for their support to prepare and publish this work. Also, we would like to thank Schlumberger for allowing the use of the Techlog software to conduct the work flow.

REFERENCES

Amer, A., Glascock, M., Schwalbach, J., Khan, M., 2011, Applied Borehole Image Analysis in Complex Sedimentological and Structural Setting: A single Well Case Study, California. Annual Technical Conference and Exhibition, Society of Petroleum Engineers, Colorado, USA. Baker Hughes, Product and Service, http://www.bakerhughes.com/products-and-services.

El Paso Exploration and Production Company "EEPC", Houston, Texas, 2011. Jurassic rift architecture in the Northeastern Western Desert, Egypt.

Goswami, J.C., Mydur, R., Wu, P., and Heliot, D. 2004, "A Robust Technique for Well-log Data Inversion," IEEE Transactions on Antennas and Propagation, pp. 717-724, March 2004

Newberry, W.M., Grace, L.M., and Stief, D.D. 2004, "Analysis of Carbonate Dual Porosity Systems from borehole Electrical Images", 1996 SPE Permian Basin Oil & Gas Recovery Conference, SPE 35158.

Newberry, B.M., Hansen, S.M., Perrett. T.T., 2010, "A Method for Analyzing Textural Changes Within Clastic Environments Utilizing Electrical Borehole Images," 2004 Gulf Coast Association of Geological Societies Transactions, Volume 54, p. 531-539.

Ramakrishna, T.S., Ramamoorthy, R., Fordham, E., Schwartz, L., Herron, M., Saito, N., and Rabaute, A 2009., "A Model-Based Interpretation Methodology for Evaluating Carbonate Reservoirs," 2001 SPE Annual Technical Conference and Exhibition, SPE 71704.

Schlumberger, 1984. "Well evaluation conference, Egypt", Schlumberger Middle East. S.A., PP.1-64.